Effect of Y_2O_3 Content on the Oxidation Behavior of Fe-Cr-Al-Based ODS Alloys

Anwar Ul-Hamid

(Submitted 3 June 2002; in revised form 19 August 2002)

A study was conducted to investigate the cyclic oxidation behavior of two oxide dispersion strengthened (ODS) Fe-Cr-Al based alloys containing 0.17 wt.% and 0.7 wt.% Y_2O_3. The alloys were oxidized in air for 100 h at 1200 °C based on a 24 h cycle period. X-ray diffraction (XRD) and analytical transmission electron microscopy (TEM) were used to characterize the structure, morphology, and composition of the oxide scales. Both alloys formed highly adherent and continuous layers of α-Al_2O_3 exhibiting a morphology indicative of inward scale growth. The role of Y_2O_3 was to promote adherence by segregating to the grain boundaries within the oxide. Concurrently, Y_2O_3 generated micro-porosity resulting in a scale of comparatively higher thickness in the alloy with 0.7 wt.% Y_2O_3.

Keywords Fe-Cr-Al, MA956, oxidation, REE, TEM, Y_2O_3

1. Introduction

Increasingly high temperatures used in industry put great demand on engineering components, especially under high stress and corrosive service environments. Oxide dispersion strengthened (ODS) alloys were developed to serve under such conditions. These alloys have the advantage of having a finely dispersed thermodynamically stable oxide phase.[1-3] The oxide dispersion present in ODS alloys show limited dissolution or coarsening, thus imparting strength to the alloys at higher temperatures. The ability of these precipitates to produce and retain a coarse-grained alloy structure results in increased creep resistance at higher temperatures,[4] as well as an improvement in the oxidation behavior.[5,6] ODS alloys are typically produced by mechanical alloying.[7]

Among ODS alloys, the Fe-Cr-Al based alloys generally outperform Ni-Cr-Al based alloys in applications that require high oxidation resistance.[3] The MA956 alloy is based on a Fe-Cr-Al system and is effectively used at temperatures exceeding 1100 °C. The matrix contains a fine dispersion of Y_2O_3, and the protection at high temperatures is provided by the formation of an α-Al_2O_3 oxide layer. The presence of Y_2O_3 dispersion not only augments the mechanical strength of the alloy, but also improves the latter's oxidation resistance by reactive element effect (REE). Several explanations have been put forward to elucidate REE on the oxidation behavior of both α-Cr_2O_3 and α-Al_2O_3 forming alloys.[8-16] The more important of these effects include a decrease in oxidation rate and an increase in scale adherence. The addition of reactive elements is also known to induce a change in the microstructure of the scale and the subscale regions.[17,18] The present study deals with the evolution of oxide scale and the effect that different Y_2O_3 concentrations have on its microstructure and consequently on oxidation behavior of the alloy.

Anwar Ul-Hamid, Materials Characterization Laboratory, Center for Engineering Research, Research Institute, King Fahd University of Petroleum and Minerals, P.O. Box 1073, Dhahran 31261, Saudi Arabia. Contact e-mail: anwar@kfupm.edu.sa.

2. Experimental Procedure

Nominal composition of INCOLOY (Special Metals Corp., Huntingdon, WV) alloy MA956 (UNS S67956) is shown in Table 1. Two MA956 alloys with 0.17 wt.% and 0.7 wt.% Y_2O_3 were used for this study. The oxidation was carried out in air for 100 h at 1200 °C on flat 20 × 10 × 2 mm specimens with 800 grit surface finish. Cross-sectional transmission electron microscopy (TEM) samples were then prepared using standard techniques[19] summarized as follows.

Each oxidized specimen was sectioned into two smaller (10 × 1.5 × 1.5 mm) pieces, which were glued together at the oxide faces. The resulting sample was then electroplated with Ni using a solution comprising 150 g $NiSO_4$, 9.5 g $NiCl_2$, 6.25 g boric acid, and 500 mL water. The solution temperature was maintained at 57 °C, while the current was kept between 0.08 and 0.12A. The sample was then sliced and ground to obtain 3 mm diameter discs having a thickness of 60 μm. The disc was dimpled and thinned to electron transparency using an ion beam miller. These samples were used to study the oxide and the scale-alloy interface viewed perpendicular to the plane of oxidation. Samples for the study of bulk alloy were prepared by jet electropolishing with a solution of 10% perchloric acid and 90% ethanol at −10 °C. The voltage and current used for polishing were 60V and 30 mA, respectively.

Microstructural characterization was carried out using TEM with an accelerating voltage of 300 kV and equipped with an energy dispersive X-ray spectroscopy (EDS) analyser. X-ray diffraction (XRD) was used for phase identification.

3. Results

3.1 Oxidation Kinetics

The weight gain data[20] showed that the alloy containing 0.7 wt.% Y_2O_3 exhibited a higher oxidation rate. It was ob-

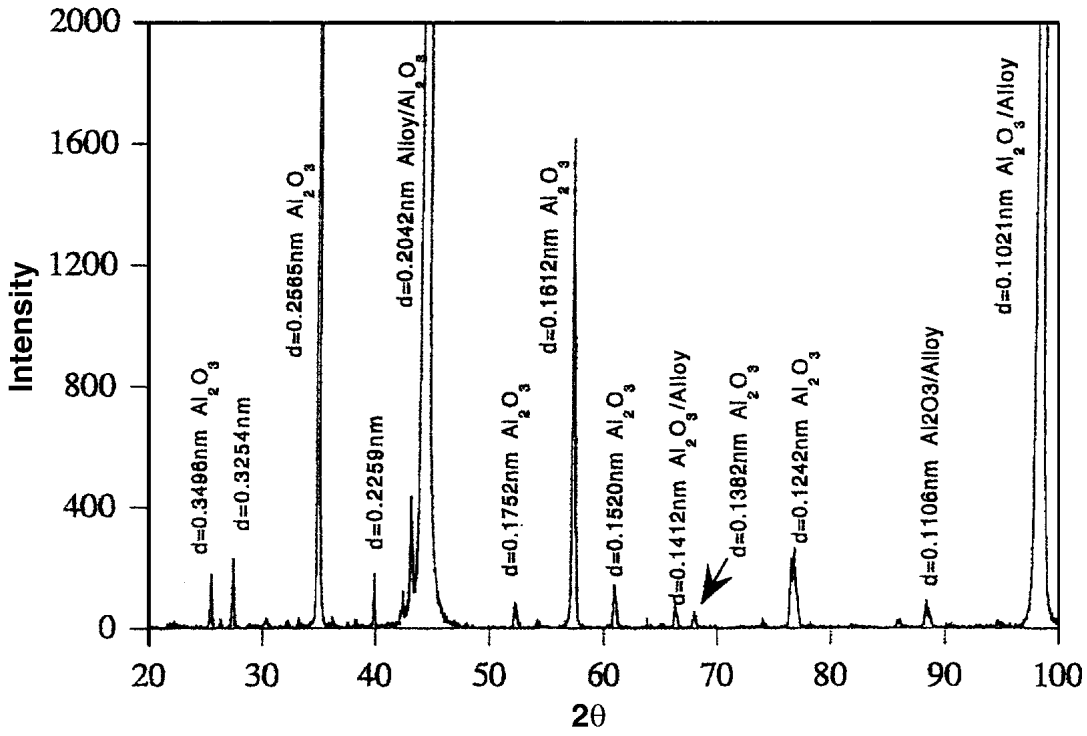

Fig. 1 X-ray diffraction spectrum obtained from the alloy with 0.7 wt.% Y_2O_3 showing prominent peaks from α-Al_2O_3 and the underlying alloy

Table 1 Nominal Composition of INCOLOY MA956 Alloy

Al	Ti	Cr	Y_2O_3	C	Cu	Mn	Co	Ni	P	Fe
3.75-5.75	0.20-0.60	18.5-21.5	0.30-0.70	0.10 max	0.15 max	0.30 max	0.30 max	0.50 max	0.02 max	Bal.

served that the difference in oxidation rates occurs at the onset of oxidation with a further increase with time.

3.2 Phase Constitution

The XRD spectrum taken from the oxidized alloy with 0.7 wt.% Y_2O_3 alloy is shown in Fig. 1. The peak with the highest diffracted intensity for the d-spacing of 0.204 nm originates from the {110} planes of the ferritic alloy. Most of the other peaks of high intensities derive from α-Al_2O_3. There was no indication for the presence of α-Cr_2O_3. Numerous low intensity peaks were observed in the spectrum, which did not belong to α-Al_2O_3 or the alloy. These peaks coincided with those expected from different Y-Al dispersoids, but no particular phase could be identified due to peak overlap. Similarly, the XRD spectrum obtained from the oxidized alloy with 0.17 wt.% Y_2O_3 exhibited α-Al_2O_3 and ferrite.

3.3 Alloy Microstructure

The MA956 alloy had a relatively coarse grained ferritic structure with an average grain size of ≈100 μm. The alloy contained fine dispersoids that varied in size from 20-700 nm, the density of dispersion being expectedly higher in the alloy with 0.7 wt.% Y_2O_3. Electron diffraction and EDS analyses showed that the dispersoids were comprised of a variety of phases. In addition, different Y-free phases were also found to form a part of the bulk microstructure.

Most of the relatively coarse (≈300-700 nm) precipitates present within the alloy were identified as titanium nitrides. An example of tetragonal Ti_2N precipitate is shown in Fig. 2(a). The EDS spectrum obtained from the same precipitate showed a high intensity Ti Kα peak at 4.56 keV (Fig. 2b). Other precipitates were identified as TiN as shown in Fig. 3(a) and (b). Another 200 nm precipitate shown in Fig. 4 was identified by electron diffraction as $AlYO_3$. Some of the finer (<30 nm) particles (see Fig. 5a) were difficult to characterize. An EDS spectrum taken from a region containing fine precipitates is shown in Fig. 5b and exhibits Y. It is thus suggested that the very fine precipitates observed in the alloy were Y-based. Different phases that can exist within Y containing Fe-Cr-Al alloys include Ti(C, N), $Y_4Al_2O_9$, $YAlO_3$, and $Y_3Al_5O_{12}$.[20]

3.4 Oxide Microstructure

Upon exposure, both MA956 alloys formed α-Al_2O_3 exclusively, as shown in Fig. 6 (a) and (b). There was no evidence for the presence of Fe or Cr based oxide, which is consistent with the XRD data presented earlier. The average thickness of the scale formed on the alloy with 0.7 wt.% Y_2O_3 was ≈8 μm

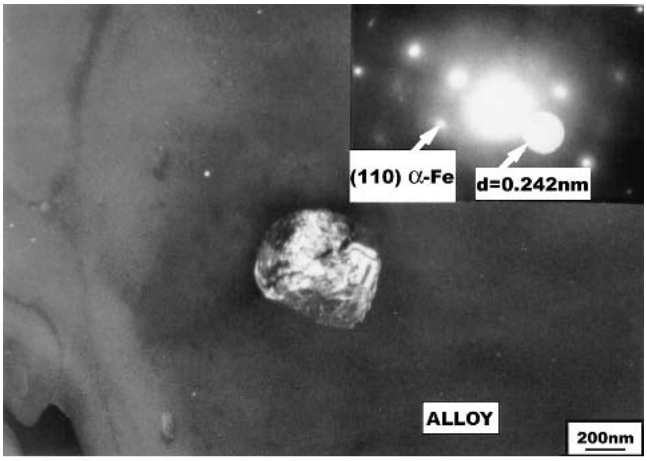

(a)

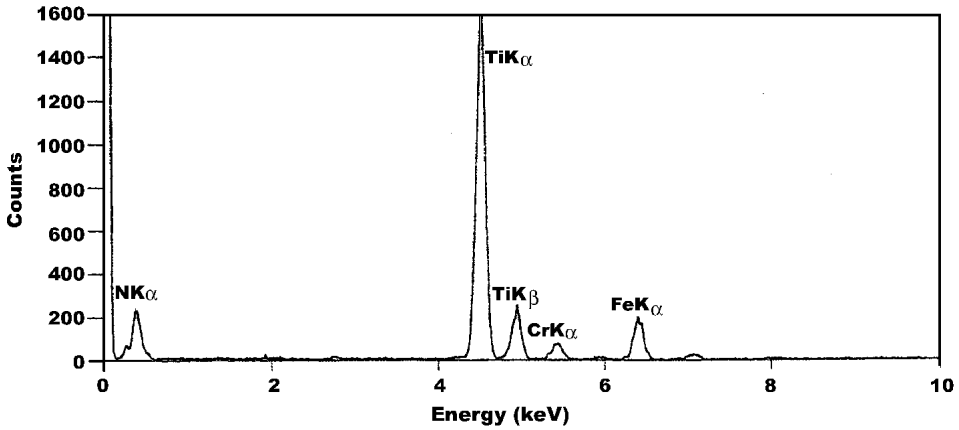

(b)

Fig. 2 **(a)** Dark field TEM micrograph showing a Ti_2N precipitate along with its diffraction pattern; **(b)** EDS spectrum obtained from Ti_2N showing a predominant Ti content

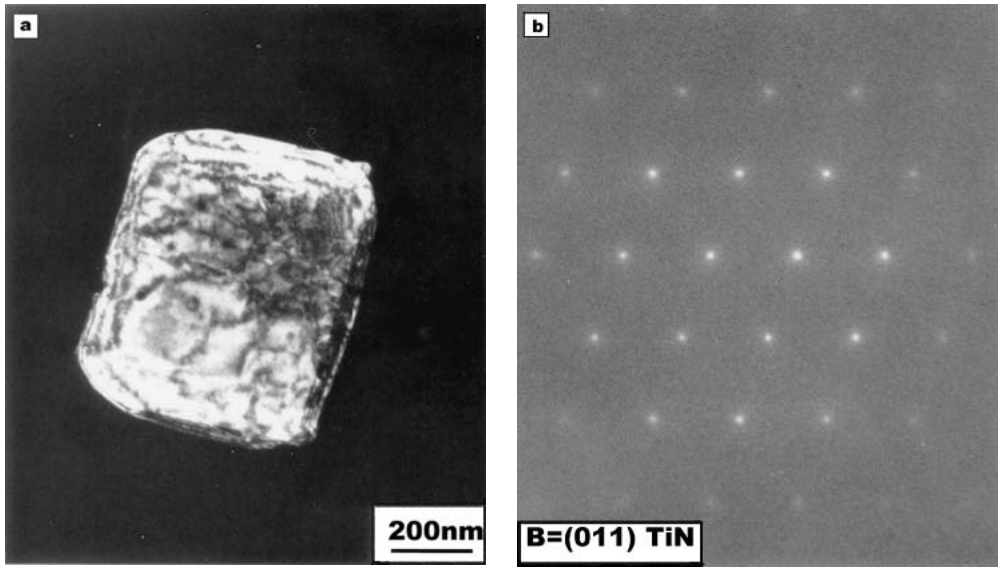

Fig. 3 **(a)** Dark field TEM micrograph showing TiN; **(b)** diffraction pattern along [011] obtained from it

compared with ≈7 μm formed on the alloy with 0.17 wt.% Y_2O_3, indicative of the higher weight gain exhibited by the former after 100 h of exposure. The scale morphology exhibited by both alloys was similar and is shown in Fig. 7.

α-Al_2O_3 exhibited a tendency to be fine and equiaxed (≈1 μm) at the scale-gas interface and coarse and columnar (Fig. 8) at the scale-alloy interface. Grain size gradually increased from the scale-gas to the scale-alloy interface so that the position at which the scale had a fine equiaxed structure is thought to be that of the original alloy surface prior to oxidation. The fine equiaxed grain formation at the upper scale surface occurs during the initial oxidation period when a large number of oxide grains nucleate and then impinge on each other to form an oxide, which has an equiaxed morphology. As oxidation proceeds, the nucleation rate of new oxide grains decreases and the existing oxide grains grow as more oxygen becomes available at the scale-alloy interface. During this competitive grain growth, some of the oxide grains are undercut by others, and the latter grow at the expense of the former and thus show an increase in size towards the scale-alloy interface. The columnar morphology of the oxide grains also indicates that oxygen diffusion has taken place through its grain boundaries.[21] New oxide is formed at the scale-alloy interface, and the original alloy surface lies near the scale-gas interface; it would appear that the scale formation on MA956 alloys had been dominated by inward oxygen diffusion.

Fig. 4 Dark field TEM micrograph of $AlYO_3$ precipitate present within the alloy

The scale-alloy interface was generally flat and even. However, a small region of the scale-alloy interface in the alloy with 0.7 wt.% Y_2O_3 (Fig. 6a) exhibited a slight inward oxide penetration. The scale at this region is ≈10 μm thick. This inward movement of a small region of the scale, though almost insignificant, is nevertheless consistent with the tendency of the Y_2O_3 modified alloys to occasionally exhibit accelerated oxidation at localized regions. The slight oxide penetration is

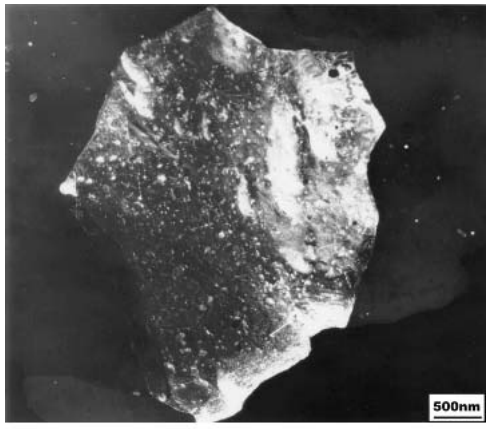

(a)

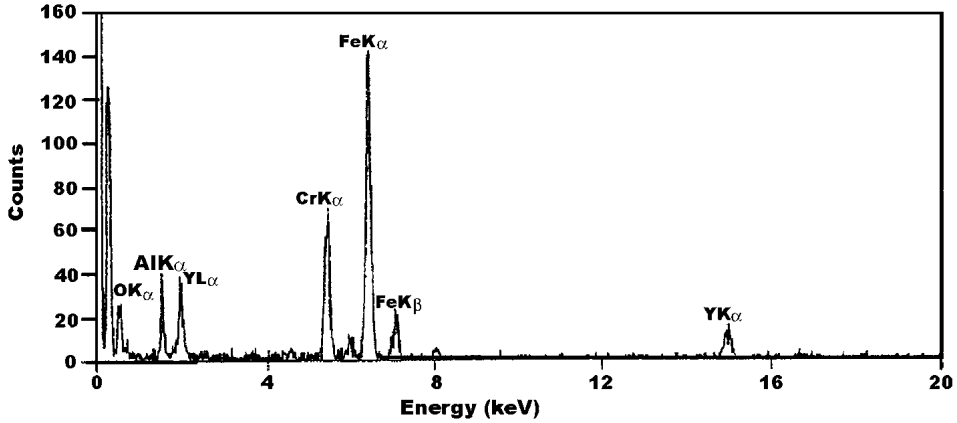

(b)

Fig. 5 **(a)** Dark field TEM micrograph of fine dispersion present within the alloy; **(b)** EDS spectrum from the fine dispersion region showing Y enrichment

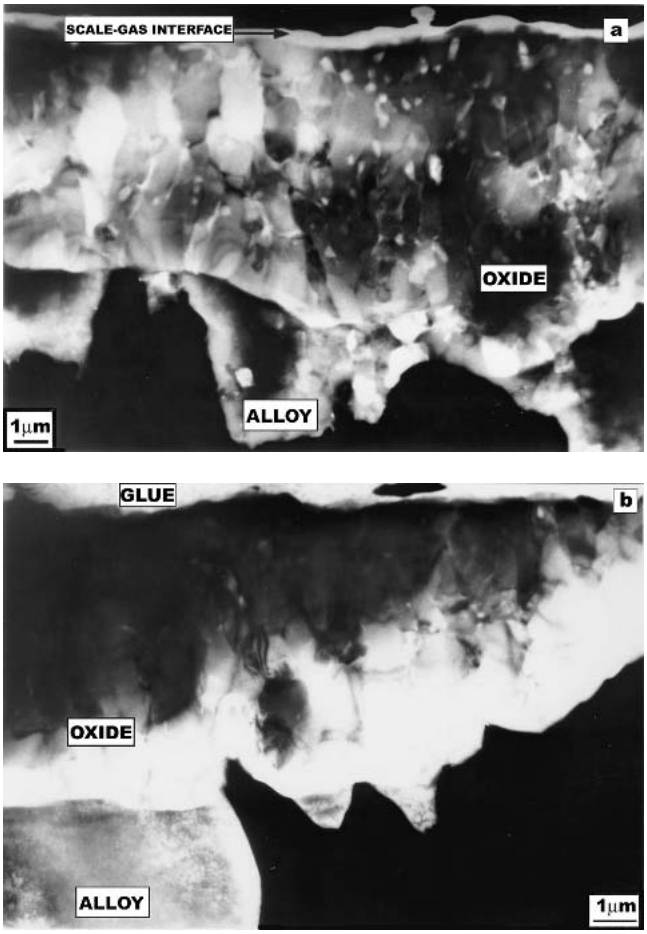

Fig. 6 **(a)** Low magnification dark field TEM micrograph of α-Al_2O_3 formed on the alloy containing 0.7 wt.% Y_2O_3; **(b)** low magnification dark field TEM micrograph of α-Al_2O_3 formed on the alloy containing 0.17 wt.% Y_2O_3

due to a relatively high concentration of dispersoids at that region.

The scale adhered to the alloy. No evidence was found of scale spallation or of the presence of coarse pores at the scale-alloy interface. However, micro-porosity existed at the scale-alloy interface, as revealed by the under- and over-focused TEM images of Fig. 9(a) and (b). The images are taken in a slightly defocused condition to accentuate the micro-pore contrast. The presence of porosity at the scale-alloy interface of an inwardly growing scale can be attributed to the condensation of excess vacancies at the interface.[22,23] The TEM images also reveal that pores are associated with the fine dispersoid particles present in the alloy immediately beneath the scale, as shown in Fig. 10(a) and (b), probably due to the loss of Y from the dispersoids to the oxide during scale growth. Pores were similarly observed within the oxide, as shown in Fig. 11(a) and (b). The oxide porosity may arise from either oxygen vacancy supersaturation or the condensation of excess Al vacancies.[24] Qualitative assessment of the results obtained in this study has revealed that the degree of porosity observed within the scale formed by the alloy with 0.7 wt.% Y_2O_3 was significantly higher than that observed in the alloy with lower Y_2O_3 content.

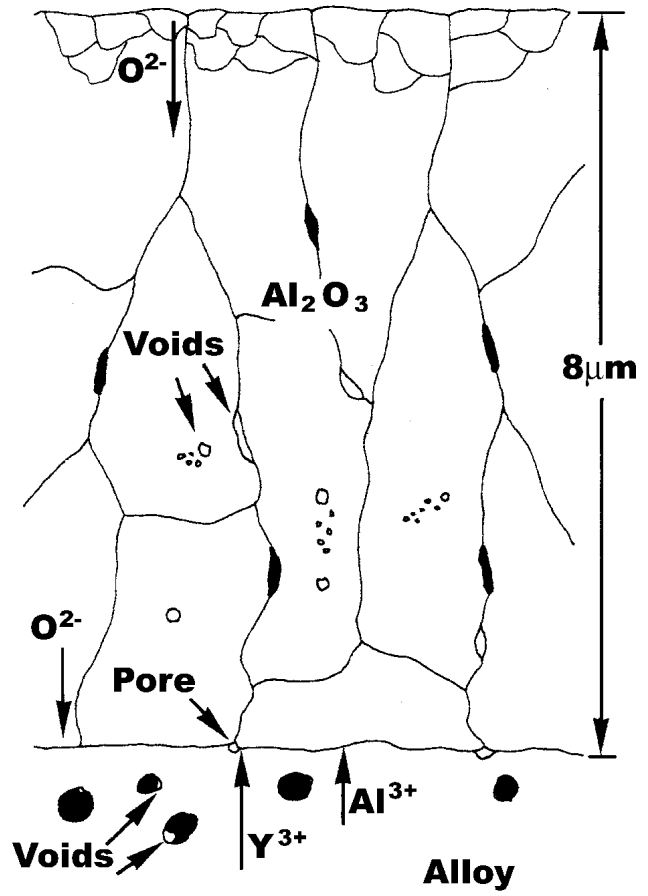

Fig. 7 Schematic illustration of the scale morphology exhibited by MA956 alloy

Fig. 8 Dark field TEM micrograph of the columnar grain morphology exhibited by α-Al_2O_3

The alloy with 0.7 wt.% Y_2O_3 also exhibited a higher presence of dispersoids within the oxide scale as shown in Fig. 12. A decrease in dispersoid density beneath the scale-alloy interface compared with the bulk alloy was observed, indicating

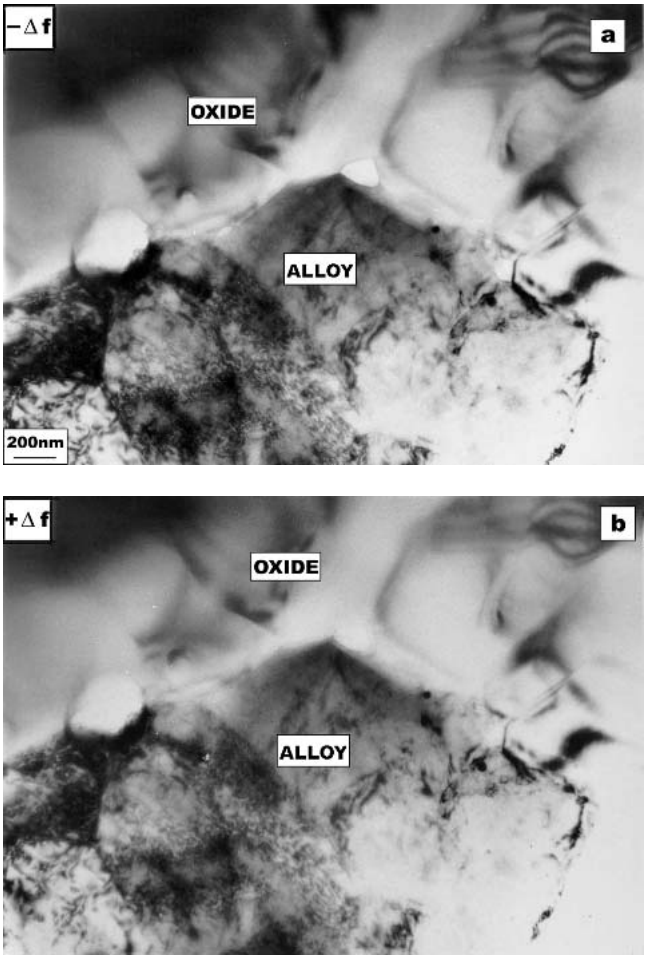

Fig. 9 Dark field TEM images of the scale-alloy interface in **(a)** under- and **(b)** over-focused condition to reveal micro-porosity

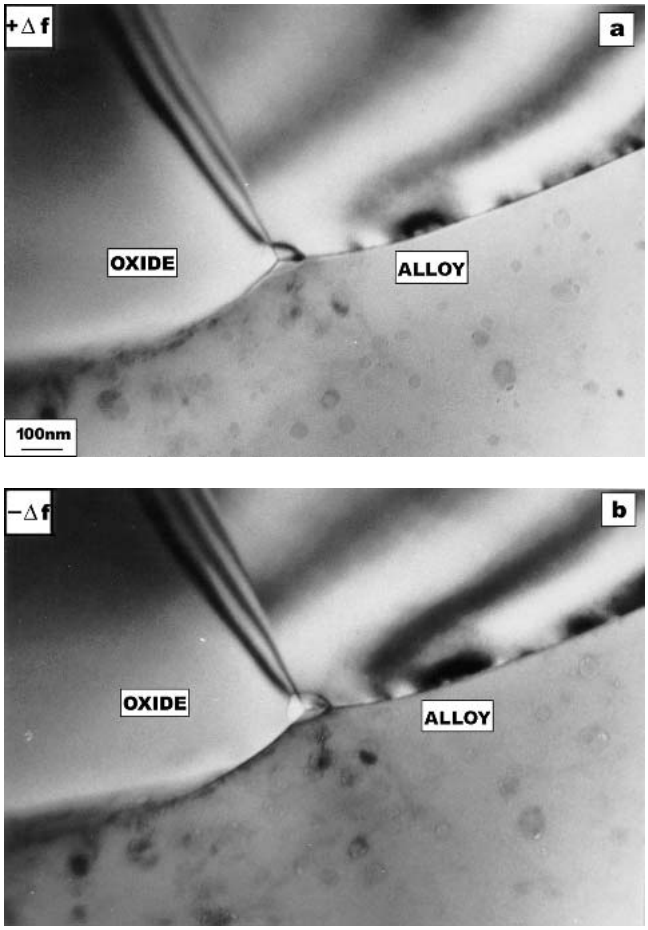

Fig. 10 Dark field TEM images of the alloy beneath the scale in **(a)** over- and **(b)** under-focused condition to reveal porosity associated with dispersoids

that the particles are getting dissolved, and Y is thus being segregated to the scale during the process of oxidation.

Elemental microanalysis at the scale-alloy interface showed presence of Y (Fig. 13a), indicating that Y segregates to the scale-alloy interface. In addition, some of the dispersoids-free oxide grain boundaries were found to be enriched in Y (Fig. 13b). The presence of Y at the oxide grain boundaries as a segregated layer suggests that dispersoids do not necessarily act as inert particles in the oxide, but they can dissociate and segregate to the oxide grain boundaries.

4. Discussion

The results of this study suggest that the scale on MA956 alloys had grown predominantly inward by oxygen diffusion. The presence of columnar grains in a relatively high volume fraction within the scale makes it highly likely for the diffusion to have occurred via oxide grain boundaries, thus suggesting it to be the predominant mechanism by which α-Al_2O_3 scale grows on this alloy.[25] This finding is consistent with the fact that the grain boundary diffusion for oxygen is greater than its bulk diffusion for doped (and undoped) α-Al_2O_3.[26]

High Y_2O_3 content of the alloy would provide a greater number of nucleation sites at the alloy surface resulting in a relatively high volume fraction of initial oxide grains. Due to the small inter-nuclei distance, the newly formed oxide grains will coalesce to form a complete layer more readily on the alloy with 0.7 wt.% Y_2O_3, resulting in a higher oxidation rate for this alloy from the onset of oxidation, which explains the initial difference in weight gain for the two alloys. The subsequent difference in the weight gain between the two alloys will depend on the difference in the rate of oxide grain growth, rather than nucleation.

Higher Y_2O_3 content alloy exhibited comparatively faster scale growth, probably due to a high degree of dispersoids and micro-porosity that serves to enhance oxygen diffusion within the scale. Dissolution of Y within the scale results in an increase in oxygen and a decrease in Al vacancy concentration. The excess Al vacancies condense at the grain boundaries, thus generating grain boundary micro-porosity.[20] Present results agree with earlier studies carried out on similar material.[20,27]

Although comparison with Y_2O_3-free alloy was not carried out in this study, it is believed that the good scale adherence exhibited by the alloys is due to the Y_2O_3 addition. Solute segregation to the oxide grain boundaries can affect the crys-

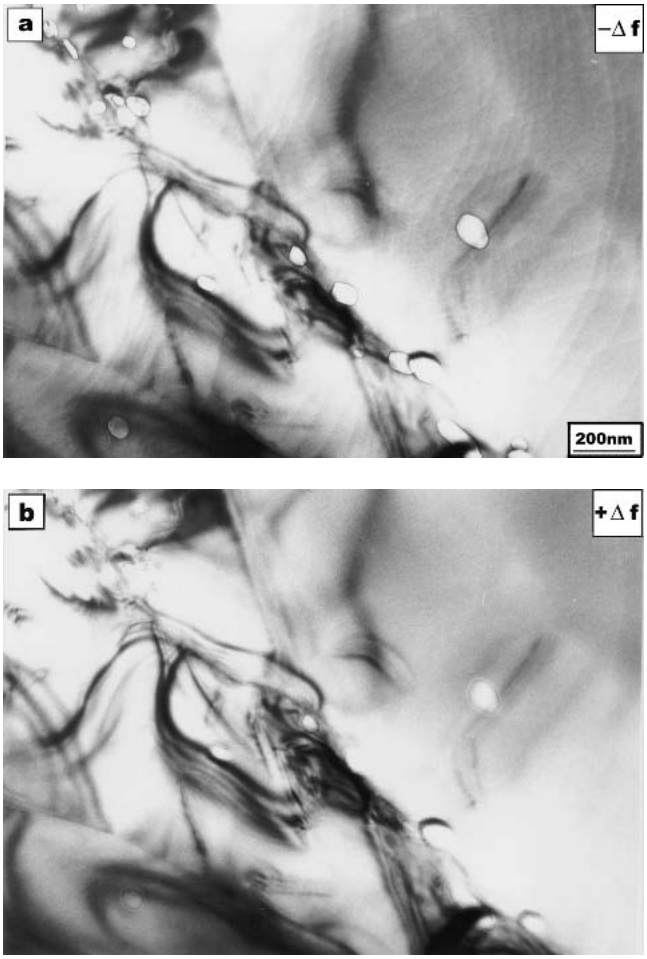

Fig. 11 Dark field TEM images of the oxide in **(a)** under- and **(b)** over-focused condition to reveal micro-porosity

tallographic orientation of oxide growth.[28] This could lead to the formation of columnar oxide grains, as observed in this study. Columnar morphology increases the fracture toughness of the scale, thus contributing towards an improved scale adherence.[25,29]

5. Conclusions

1) α-Al_2O_3 formed on an ODS Fe-Cr-Al alloy grows predominantly by inward oxygen diffusion through the oxide grain boundaries and is highly adherent to the alloy.
2) High Y_2O_3 content in the alloy gives rise to a high degree of porosity within the scale, resulting in a relatively high scale growth rate. The porosity is thought to form due to Y-doping of the scale.

Acknowledgments

I am thankful to Drs. A. Czyrska-Filemonowicz and S.B. Newcomb for the provision of material and advice. I am grateful to Cambridge Commonwealth and Newton Trusts for the provision of sponsorship and research grants. Thanks are also due to the Department of Materials Science and Metallurgy, University of Cambridge, England, and the Research Institute at King Fahd University of Petroleum and Minerals, Saudi Arabia, where this work was carried out.

Fig. 12 TEM micrograph showing the presence of a dispersoid particle within the oxide scale

References

1. J.S. Benjamin: *Metall. Trans.*, 1, 1970, p. 2943.
2. G. Korb and A. Schwaiger: *High Temperatures High Pressures*, 1989, *21*, p. 475.
3. W.J. Quadakkers: *J. De Physique*, 1993, *IV*(C9 3), p. 177.
4. E. Grundy and W.H. Patton: *High Temperature Alloys: Their Exploitable Potential*, Commission of the European Communities, J.B. Marriot, M. Merz, J. Nihoul, and J. Ward, ed., Elsevier, London, 1985, p. 327.
5. W.J. Quadakkers, H. Holzbrecher, K.G. Briefs, and H. Beske: *Oxid. Met.*, 1989, *32*, p. 67.
6. M.J. Bennett, H. Romary, and J.B. Price: *Heat Resistant Materials*, ASM International, Materials Park, OH, 1991, p. 95.
7. H. Hedrich: *New Materials by Mechanical Alloying Techniques*, E. Artz and L. Schulz, ed., Deutsche Gesellschaft für Materialkunde, Frankfurt, Germany, 1990, p. 227.
8. D.P. Whittle and J. Stringer: *Phil. Trans. R. Soc. Lond.*, 1980, *A295,* p. 309.
9. F.H. Stott: *Rep. Prog. Phys.*, 1987, *50,* p. 861.
10. K. Przybylski and G.J. Yurek: *Mater. Sci. Forum*, 1989, *43*, p. 1.
11. J. Jedlinski: *Solid State Phenomenon*, 1992, *21/22,* p. 335.
12. G.C. Wood and F.H. Stott: *High Temperature Corrosion*, R.A. Rapp, ed., NACE-6, Houston, TX, 1983, p. 227.
13. H.M. Hindam and D.P. Whittle: *Oxid. Met*., 1982, *18*(5/6), p. 245.
14. A.M. Huntz: *The Role of Active Elements in the Oxidation Behavior of Metals and Alloys*, E. Lang, ed., Elsevier Applied Science, London/New York, 1989, p. 81.
15. A.M. Huntz: *Mater. Sci. Eng*., 1987, *87*, p. 251.
16. F.H. Stott and G.C. Wood: *Mater. Sci. Eng*., 1987, *87*, p. 267.
17. J. Stringer, B.A. Wilcox, and R.I. Jaffe: *Oxid. Met.*, 1972, *5,* p. 11.
18. O.T. Goncel, J. Stringer, and D.P. Whittle: *Corros. Sci.*, 1978, *18,* p. 701.
19. S.B. Newcomb, C.B. Boothroyd, and W.M. Stobbs: *J. Microsc*., 1985, *140,* p. 195.
20. A. Czyrska-Filemonowicz, R.A. Versaci, D. Clemens, and W.J. Quadakkers: *Microscopy of Oxidation*, 2, S.B. Newcomb and M.J. Bennett, ed., Institute of Materials, London, UK, 1993, p. 288.

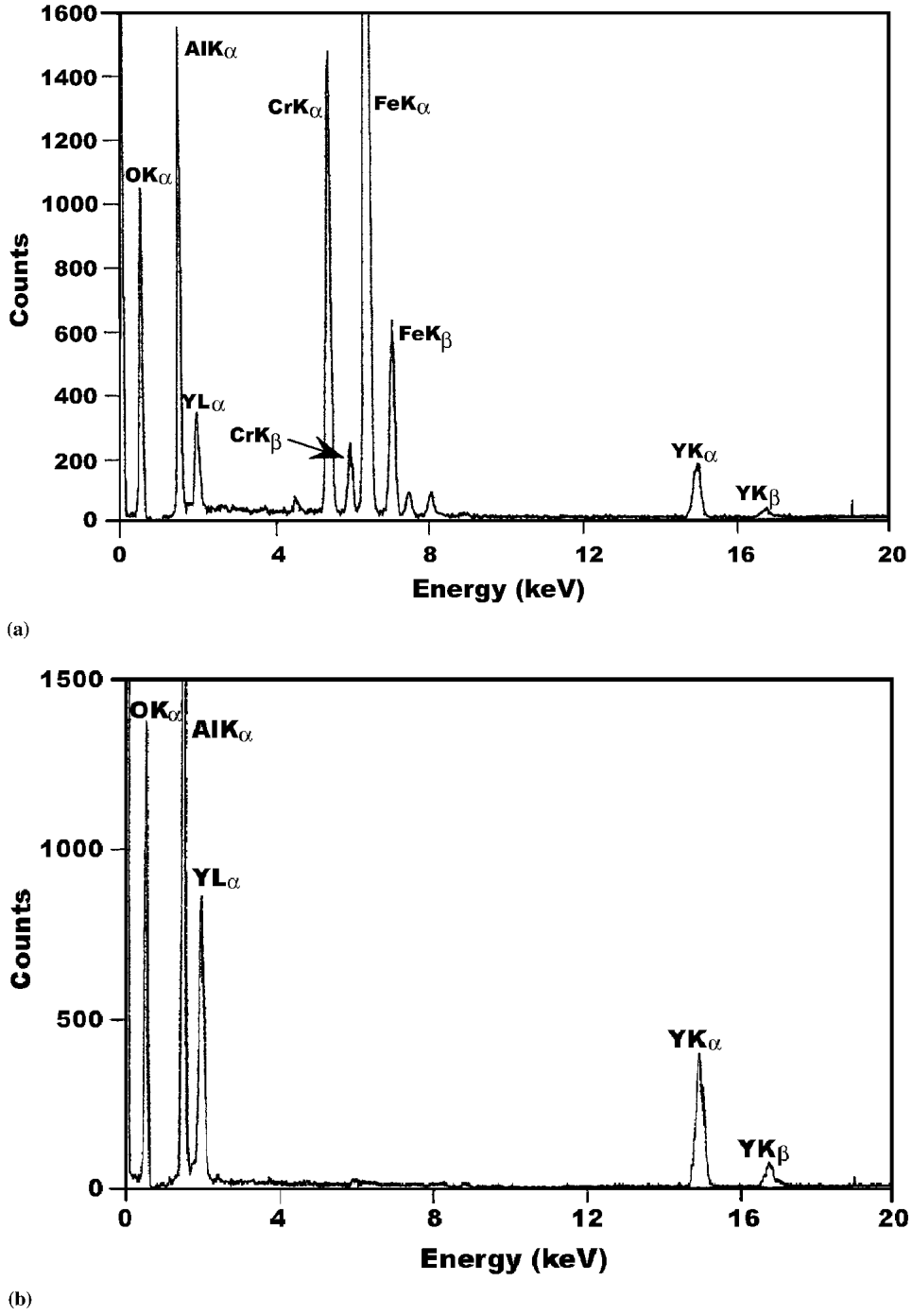

Fig. 13 **(a)** EDS spectrum obtained from the scale-alloy interface showing the presence of Y; **(b)** EDS spectrum obtained from the oxide grain boundary showing the presence of Y

21. D.P. Whittle and H.M. Hindham: *Corrosion-Erosion-Wear of Materials in Emerging Energy Systems*, NACE, Houston, TX, 1982, p. 54.
22. J.D. Kuenzly and D.L. Douglass: *Oxid. Met.*, 1974, *8*(3), p. 139.
23. A. Kumar, M. Nasrallah, and D.L. Douglas: *Oxid. Met.*, 1974, *8*(4), p. 227.
24. T.A. Ramanarayanan, M. Raghavan, and R. Petkovic-Luton: *J. Electrochem Soc.,* 1984, *131*, p. 923.
25. T.A. Ramanarayanan, R. Ayer, R. Petkovic-Luton, and D.P. Leta: *Oxid. Met.*, 1988, *29*(5/6), p. 445.
26. M. Le Gall, B. Lesage, C. Monty, and J. Bernardini: *J. Mater. Sci.*, *30*, 1995, p. 201.
27. A. Czyrska-Filemonowicz and B. Dubiel: *J. Mat. Processing Tech.*, 1997, *64,* pp. 53-64.
28. D.A. Smith, C.M.F. Rae, and C.M. Grovenor: *Grain Boundary Structure and Kinetics*, ASM Materials Science Seminar, ASM, Metals Park, OH, 1980, p. 350.
29. K.T. Faber and A.G. Evans: *Acta Met.*, 1983, *31*, pp. 565-77.